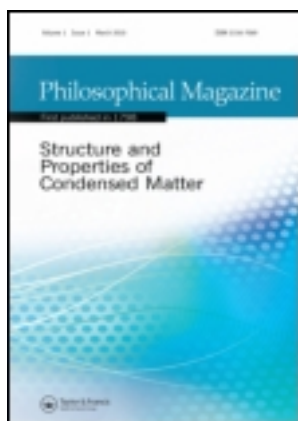


This article was downloaded by: [Institute of Metals Research]

On: 13 January 2013, At: 16:41

Publisher: Taylor & Francis

Informa Ltd Registered in England and Wales Registered Number: 1072954 Registered office: Mortimer House, 37-41 Mortimer Street, London W1T 3JH, UK



Philosophical Magazine

Publication details, including instructions for authors and subscription information:

<http://www.tandfonline.com/loi/tphm20>

Microstructure of the potentially multiferroic Fe/BaTiO₃ epitaxial interface

X. Wang^a, Y.L. Zhu^a, X.W. Wang^a, Y.Q. Zhang^a & X.L. Ma^a

^a Shenyang National Laboratory for Materials Science, Institute of Metal Research, Chinese Academy of Sciences, Shenyang 110016, China

Version of record first published: 22 Feb 2012.

To cite this article: X. Wang, Y.L. Zhu, X.W. Wang, Y.Q. Zhang & X.L. Ma (2012): Microstructure of the potentially multiferroic Fe/BaTiO₃ epitaxial interface, *Philosophical Magazine*, 92:14, 1733-1747

To link to this article: <http://dx.doi.org/10.1080/14786435.2012.657709>

PLEASE SCROLL DOWN FOR ARTICLE

Full terms and conditions of use: <http://www.tandfonline.com/page/terms-and-conditions>

This article may be used for research, teaching, and private study purposes. Any substantial or systematic reproduction, redistribution, reselling, loan, sub-licensing, systematic supply, or distribution in any form to anyone is expressly forbidden.

The publisher does not give any warranty express or implied or make any representation that the contents will be complete or accurate or up to date. The accuracy of any instructions, formulae, and drug doses should be independently verified with primary sources. The publisher shall not be liable for any loss, actions, claims, proceedings, demand, or costs or damages whatsoever or howsoever caused arising directly or indirectly in connection with or arising out of the use of this material.

Microstructure of the potentially multiferroic Fe/BaTiO₃ epitaxial interface

X. Wang, Y.L. Zhu*, X.W. Wang, Y.Q. Zhang and X.L. Ma

*Shenyang National Laboratory for Materials Science, Institute of Metal Research,
Chinese Academy of Sciences, Shenyang 110016, China*

(Received 9 November 2011; final version received 10 January 2012)

The Fe/BaTiO₃ thin-film layered structure is a prototype of charge-mediated composite multiferroics, which is a promising but challenging route to achieve a sizable magnetoelectric effect. The real structure of the interface between the ferromagnetic Fe and ferroelectric BaTiO₃ layers is crucial. In this paper, epitaxial Fe layers were successfully grown on top of BaTiO₃ layers by carefully controlling the pulsed laser deposition and magnetron sputtering procedures. A detailed study of interfacial structure and defects at the Fe/BaTiO₃ interface was carried out by transmission electron microscopy (TEM). Electron diffraction patterns and diffraction contrast images reveal a definite epitaxial relationship between Fe and BaTiO₃ (001) films and a semi-coherent interface with nearly periodic interfacial dislocations. Based on high-resolution TEM images from both [010] and [110] direction observations, the interfacial dislocations were found to be partial with Burgers vectors $\frac{1}{2}a(100)$ and line directions of $\langle 010 \rangle$. By employing high-resolution Z-contrast imaging, the positions of individual atoms columns were resolved. The formation mechanism of interfacial dislocations was proposed in terms of geometrical models of the interface structure. On the basis of the remaining strain analysis in each layer, the effects of both BaTiO₃ thickness and the SrTiO₃ substrates on the density of the interface defects were discussed.

Keywords: multilayer thin films; epitaxial growth; interface structure; high-resolution electron microscopy; composite multiferroics

1. Introduction

The electrical control of magnetism is an important field of research due to its possible application in information storage media and spintronics [1]. Single-phase multiferroic material, such as BiFeO₃, REMnO₃, LuFe₂O₄ or TbMnO₃ [2–5], which simultaneously possess two or more ferroic properties, i.e. ferroelectricity, ferromagnetism, ferrotoroidic and ferroelasticity [1,6,7], may be possible choices. Unfortunately, there are very few single-phase multiferroic materials and coupling between magnetism and electricity in intrinsic multiferroics is rare and weak [8–10]. Despite ongoing research for new single-phase multiferroics, the concept of exploring proximity and interfacial effects by combining ferromagnetic and ferroelectric phases

*Corresponding author. Email: ylzhu@imr.ac.cn

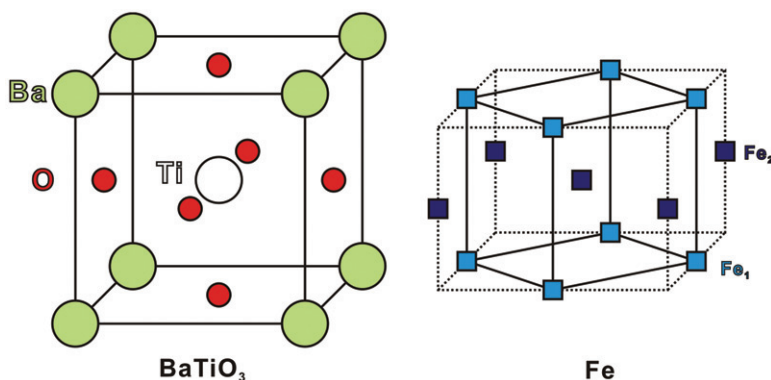


Figure 1. Schematic drawings of the unit cell of BTO and Fe.

to achieving large magnetoelectric coupling has been proposed and developed as an alternative [11–13]. Composite structures take advantage of a specific coupling between the individual components and offer an attractive approach to the design of new materials. Based on this concept, a number of strategies have been considered, such as strain-mediated [11,13], exchange-bias-mediated or charge-mediated [14] etc. Among them, the charge-mediated approach, which was first suggested by theoretical calculations, is a new direction in the field of magnetoelectric coupling and has been less well explored [14].

The Fe/BaTiO₃ system is a good first choice when studying the charge-mediated magnetoelectric coupling effect for several reasons. First, Fe and BaTiO₃ are, respectively, classical ferromagnetic and ferroelectric materials in bulk. Second, the mismatch between bcc Fe and perovskite BaTiO₃ with a 45° rotation of its cubic lattice is relatively small (only 1.4%), as shown in Figure 1. This makes it possible to fabricate Fe/BaTiO₃ heterostructures epitaxially and to couple the two ferroic orders through the interface. To date, some first principles calculations have been performed predicting an interface magnetoelectric response in Fe/BaTiO₃ heterostructures as large as that induced by strain, which was attributed to changes in chemical bonding at the ferroelectric-ferromagnetic interface [15,16]. Another mechanism which was also predicted to induce sizable interface magnetoelectric coupling in this structure is spin-dependent electron screening [17,18]. Changing the direction of ferroelectric polarisation influences not only interfacial magnetisation and anisotropy, but also spin polarisation at the interface, while spin polarisation is the key parameter controlling the response of spintronic systems. Recently, Garcia et al. [19] investigated the non-volatile electrical control of spin polarisation by preparing multiferroic tunnel junctions of Fe/BaTiO₃/La_{0.67}Sr_{0.33}MnO₃ multilayer. Spin polarisation of electron tunnelling from the Fe electrode through ultrathin ferroelectric BaTiO₃ tunnel barriers was observed. This experimentally demonstrated a charge-mediated magnetoelectric coupling in heterostructures for the first time [19].

However, the epitaxial growth of the Fe/BaTiO₃ heterostructures has been rarely reported, because the film growth of a metal or an oxide needs different conditions and is difficult to control simultaneously. This is one of the most important

challenges in the study of the magnetoelectric coupling effect in this type of heterostructure. Only recently, Brivio et al. [20] reported the epitaxial growth of Fe on BaTiO₃ thin films, but they detected an interfacial oxidised layer with a thickness of 3 nm in Fe films. In this paper, we report an epitaxial relationship between Fe and BaTiO₃ in Fe/BaTiO₃ multilayer films grown on SrTiO₃ (001) substrates, which conforms to the structure assumptions on which the theoretical calculations are based [15–18]. The oxidation of iron near the interface was absent within the detection limits in the present study.

In addition, there is a paucity of detailed structure information on the Fe/BaTiO₃ interface. Meyerheim et al. [21] reported the geometric structure of ultrathin BaTiO₃ films on Fe (001). The method they used, however, to study the structure was surface X-ray diffraction, which only provides structural information in the reciprocal space in general. From another study, the thickness of the BaTiO₃ layer was restricted to 1–3 unit cells, which is far less than the ferroelectric critical thickness of BaTiO₃ films [22]. Transmission electron microscopy (TEM), which is able to provide a direct, local interpretation of chemical and structural information of the interface on an atomic scale, is a very powerful tool to investigate interfacial structures, especially in studying the strain and defects in thin films and interfaces [23–26]. Here, we present a detailed structural investigation on the epitaxial interface between Fe and BaTiO₃ by TEM. The character and configuration of misfit dislocation networks at the interfaces are interpreted, and the thickness-dependent density of interfacial defects is discussed from the viewpoint of the misfit strain.

2. Experimental procedure

Pulsed laser deposition (PLD) and magnetron sputtering were combined to grow the layered composite multiferroic Fe/BaTiO₃ thin films. Prior to BaTiO₃ film growth, the SrTiO₃ (001) substrates were cleaned in an ultrasonic bath with acetone followed by ethanol. Then, the substrates were heated to 750°C and kept for about 5 min in the PLD chamber to evaporate surface contaminants. After that, three BaTiO₃ thin films with thicknesses of 2, 3 and 6 nm were grown by PLD, employing a KrF excimer laser ($\lambda = 248$ nm) with a repetition rate of 2 Hz and a flux of approximately 0.6 J/cm². The growth temperature and the oxygen pressure during BaTiO₃ growth were optimised at 750°C and 30 Pa. To acquire high-quality epitaxial BaTiO₃ thin films and flat BaTiO₃ surfaces, the samples were post-annealed at the growth temperature for 15 min and then cooled at a rate of 25°C/min. Subsequently, the samples were transferred to the magnetron sputtering chamber. Using magnetron sputtering, iron layers of 10 nm in thickness were deposited on top of the as-received BaTiO₃ layers in an Ar gas atmosphere. The growth temperature was optimised at 200°C and the growth rate was about 0.22 Å/s. After Fe deposition, a Pt layer of about 3 nm thickness was grown on top of the Fe layer as a protective layer to prevent the oxidation of Fe.

Cross-sectional TEM specimens with both [010] and [110] viewing directions of the substrates were prepared by conventional method, i.e. slicing, grinding, dimpling and finally ion-milling. A Gatan precision ion polishing system (PIPS) with a liquid nitrogen-cooled stage was used to prevent the cross-sectional specimens from

preference thinning. A Tecnai G² F30 transmission electron microscope (FEI), equipped with a high-angle annular dark-field (HAADF) detector was used for selected area electron diffraction (SAED), bright-field imaging, high-resolution transmission electron microscopy (HRTEM) and Z-contrast imaging. The accelerating voltage of the electron microscope was 300 kV and the spherical aberration coefficient was 1.2 mm. The point-to-point resolution was 0.203 nm with information limits of 0.14 nm.

3. Results

3.1. Epitaxial growth of Fe layer on BaTiO₃ thin films

After optimizing the growth conditions of both Fe and BaTiO₃ (BTO) thin films and keeping the surface clean during the film growth process, Fe layers were found to grow epitaxially on all three BTO thin films. Figure 2 is a typical cross-sectional SAED pattern of the Fe/BTO thin films on the SrTiO₃ (STO) substrate taken from the area covering both the films and substrates. Figure 2a is the [010] zone axis of STO; whereas Figure 2b is the [110] zone axis. The strong spots in the patterns are diffractions from STO, while the weak spots accompanying the strong ones are from BTO, as marked by short arrows in Figure 2a and b, respectively. Because BTO shares a similar lattice with STO, but with larger lattice parameters and an elongate *c* axis, spot splitting due to the difference in lattice parameters of BTO and STO is obvious. The superposed EDPs of BTO and STO demonstrate the single crystalline quality of BTO and an epitaxial relationship between BTO and STO. In addition these basic spots, extra spots also appear, as marked by a white rectangle and rhombus, in Figure 2a and b, respectively. These spots can be indexed as the set of Fe lattice. The superposed EDPs of BTO and Fe are direct evidence of the epitaxial growth of Fe on the BTO film surface from these two viewing directions.

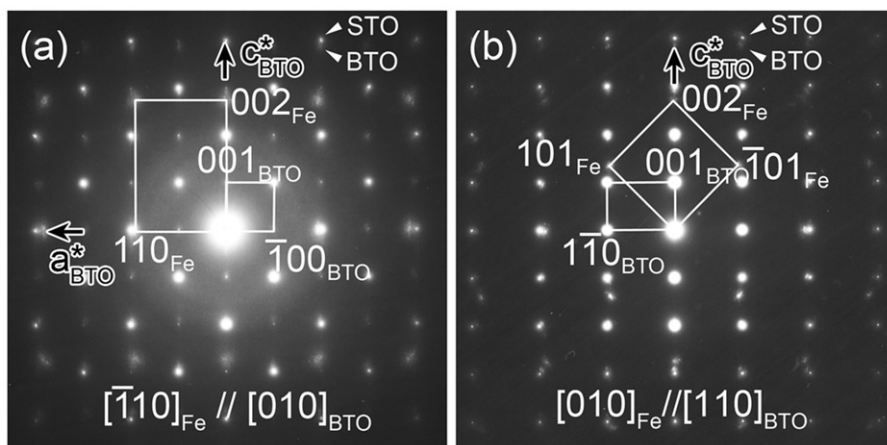


Figure 2. Cross-sectional electron diffraction patterns of the Fe/BTO films grown on STO (001) substrates taken along the (a) [010] and (b) [110] direction of STO, showing the epitaxial relationship between Fe and BTO.

The epitaxial relationships between Fe and BTO are concluded to be $(001)_{\text{Fe}} \parallel (001)_{\text{BTO}}$ and $[\bar{1}10]_{\text{Fe}} \parallel [010]_{\text{BTO}}$, i.e. the Fe lattice grows in the $[001]$ direction of BTO, and the $[100]$ and $[010]$ axes of the cubic Fe lattice rotated 45° with respect to the tetragonal BTO lattice along the $[001]$ growth direction. For convenience, the indices of the directions and planes in this paper are based on the set of STO or BTO, if not specified.

To investigate the interface structure evolution with the thickness of BTO layers, the lattice constants of BTO (c and a), the values of volume^{1/3} and c/a ratio were measured and calculated on the basis of the superposed EDPs for Fe/BTO hetero films with different BTO thicknesses. In the measurements, the lattice constants were calibrated by the bulk lattice parameter of STO of $a=0.3905$ nm. The results are shown in Figure 3. Bulk values based on the data in JCPDS cards were drawn by horizontal lines for reference purposes. The shadowed area denotes the critical thickness region for BTO films on the STO substrate obtained by theoretical calculations, above which the strain in BTO films induced by mismatch from the STO substrate will start to relax theoretically. For films grown with BTO thicknesses of 2, 3 and 6 nm, the out-of-plane parameters c are larger than the in-plane parameters to some extent, as shown in Figure 3a and c, i.e. all the BTO films are c -axis oriented tetragonal. Below the critical thickness, due to the effects of the STO substrate, the a parameters of 2 and 3 nm thick BTO films are constrained to be close to the lattice parameter of STO (0.3905 nm), while the c parameter is elongated to be

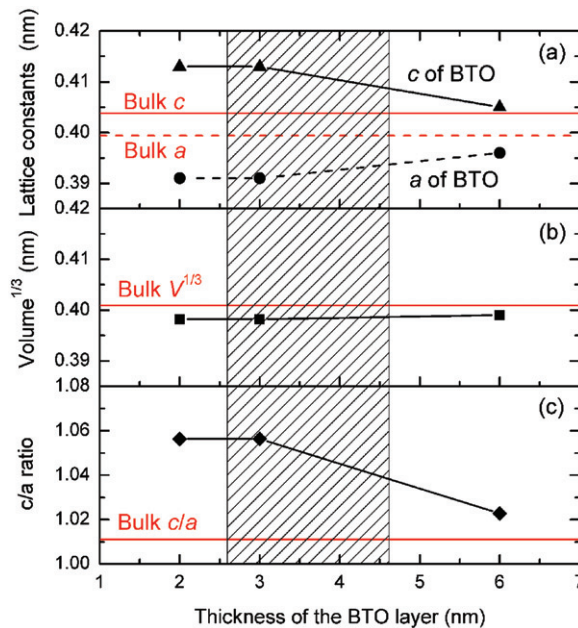


Figure 3. Variations in (a) the a and c lattice constants, (b) the value of volume^{1/3}, and (c) the c/a ratio of the BTO layers with changes in the thickness of the BTO layer. The horizontal lines denote the bulk values and the shadowed area denote the critical thickness region of single layer BTO films deduced from the theory.

$c \approx 0.413$ nm. This indicates that the BTO films are totally strained by the substrates at these two thicknesses. When the BTO thickness increases above the critical thickness and up to 6 nm, both a and c approach the bulk values, which means that the misfit strain in 6-nm thick BTO films is released to some extent and, consequently, the tetragonality decreases. Figure 3b is a plot illustrating that the unit cell volumes remain nearly constant for all thicknesses and are slightly smaller than the bulk values. This may be an indication of few oxygen vacancies, introduced during film growth under high oxygen pressure, being available in our BTO films. Note that it has been reported that oxygen vacancies in BTO can induce volume expansion [27,28]. Nevertheless, substrate clamping on the BTO films, especially when the thickness of BTO is very thin, may also cause shrinkage of the lattice volume. BTO films would adopt the structure of STO, when the thickness of BTO is very thin.

As the strain state of the BTO films changes the lattice parameters of the BTO thin films, it consequently affects the lattice mismatch of the interface between Fe and BTO. Figure 4 shows the in-plane lattice constants of both Fe and BTO in the films and the mismatch between them with the variation in BTO films thickness. The mismatch is 4.3% for totally strained BTO films and 3.0% for partially relaxed films, which is obviously larger than the mismatch between Fe and the unstrained BTO (1.42%).

3.2. Character determination of the dislocations at Fe/BaTiO₃ interface

Figure 5 shows bright-field cross-sectional TEM images of the Fe/BTO multilayer films on STO substrate with a 2-nm thick BTO layer taken under $g = [100]$ and $[001]$ two-beam conditions, respectively. The transverse arrows denote the interfaces of

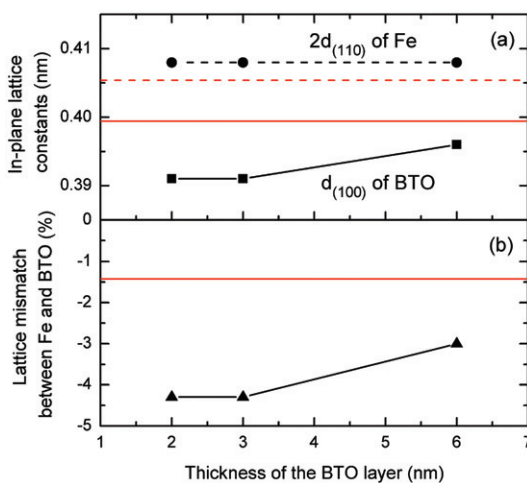


Figure 4. Variations in (a) the in-plane lattice constants of Fe and BTO, and (b) the lattice mismatch between them with changes in the thickness of the BTO layer. The horizontal lines denote the bulk values.

BTO/STO, Fe/BTO, and Pt/Fe from bottom to top, respectively. No dislocation is present at the BTO/STO interface in Figure 5a, which means that the BTO film is totally strained, and is in accordance with the EDPs result above. As expected, for the films with a BTO thickness exceeding the critical thickness (images not shown), some dislocations can be found at the BTO/STO interface. In contrast, high density interfacial dislocations were observed at regular intervals along the Fe/BTO interface in all films with different BTO thickness. They exhibited dark dot contrast as denoted by vertical arrows, which indicates that the dislocation lines are imaged end-on in the [010] projection. These interfacial dislocations do not exhibit contrast in the $g=[001]$ two-beam condition, as shown in Figure 5b. This implies that the Burgers vectors of these interfacial dislocations do not contain the [001] component. These interfacial dislocations have Burgers vectors parallel to the interface, and contribute to the misfit relaxation. Therefore, they are misfit dislocations (MDs).

HRTEM imaging was operated to further investigate the characters of these interfacial dislocations at the Fe/BTO interface. Figure 6a–c are typical cross-sectional HRTEM images showing these interfacial dislocation configurations taken along the [010] and [110] directions, respectively. As shown in Figure 6a, the dislocation looks more atomically sharp in [010] projection, implying that the dislocation line direction may be along the [010] direction, which matches well with the diffraction contrast results shown in Figure 5a and b. By tracing Burgers circuits surrounding the dislocations, the projection components of the Burgers vectors of the dislocations on the two image planes can be determined. In our work, the component of the Burgers vectors in [010] projection was determined to be $\frac{a}{2}[\bar{1}00]$, while the component in [110] projection was determined to be $\frac{a}{4}[\bar{1}10]$, as shown in Figure 6a and b, respectively. Then, the real full Burgers vectors of these dislocations

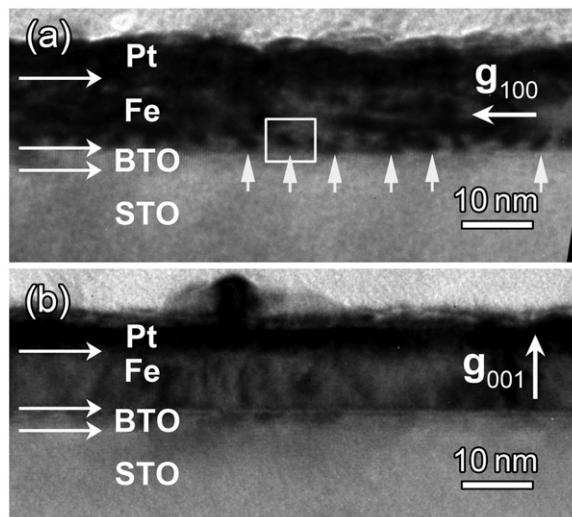


Figure 5. Low-magnification bright-field cross-sectional TEM images of the interfacial dislocation array at the Fe/BTO interface taken under (a) $g=[100]$ and (b) $[001]$ two-beam conditions.

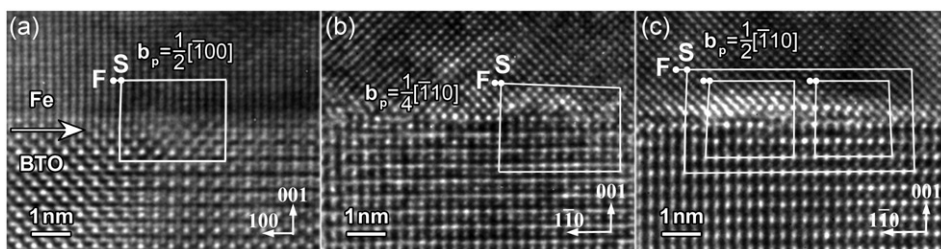


Figure 6. HRTEM images taken along the directions of (a) [010] and (b and c) [110], showing the projections of the Burgers vectors of the interfacial dislocations along the corresponding directions.

can be determined on the basis of the measured projections. From Figure 6a, the Burgers vector in [010] projection is $\frac{a}{2}[\bar{1}00]$. According to the association between real Burgers vectors and projection components of Burgers vector summarised in Jia's paper [23], the true Burgers vector may be $\frac{a}{2}[\bar{1}00]$, $\frac{a}{2}[\bar{1}10]$ or $\frac{a}{2}[\bar{1}\bar{1}0]$. In all three possible Burger vectors proposed above, only the $\frac{a}{2}[\bar{1}00]$ vector has the projection components of $\frac{a}{4}[\bar{1}10]$, as identified in Figure 6b. In addition to the case in Figure 6b, the dislocation with $\frac{a}{4}[\bar{1}10]$ Burgers vector component was occasionally identified in [110] projection, as shown in Figure 6c. Because the distortion region of this kind of dislocation is relatively larger than other dislocations, two decomposed dislocations with $\frac{a}{4}[\bar{1}10]$ Burgers vector components in [110] projection can be deduced, as in the case shown in Figure 6c where two small Burgers circuits were drawn. Summarizing all the results above, the majority of the interfacial dislocations are concluded to be edge dislocations with Burgers vectors of $\frac{a}{2}[\bar{1}00]$ in the BTO lattice, i.e. $\frac{a_{Fe}}{2}[\bar{1}\bar{1}0]$ in the Fe lattice, following the epitaxial relationship determined above. This Burgers vector corresponds to the partial dislocations of bulk BTO and Fe. Thus, these dislocations will change the translation state and also the interface atomic structure at coherent region on both sides.

In comparison with coherent HRTEM imaging, incoherent HAADF Z-contrast imaging with atomic differentiation can provide detailed chemical information of the interface at an atomic level. Figure 7 is a cross-sectional high-resolution HAADF image of the Fe/BTO interface area in the Fe/BTO films with a 2-nm thick BTO layer viewed along the [010] direction. Only $(110)_{Fe}$ lattice planes with a spacing of 0.203 nm are visible in the Fe crystal. The $(002)_{Fe}$ lattice planes (perpendicular to $(110)_{Fe}$) possess a spacing of 0.143 nm, which is beyond the resolution limit of our microscope. By checking the continuity of the lattice plane perpendicular to the Fe/BTO interface from both upper and lower sides, the dislocation positions were located, as denoted by perpendicular white lines drawn in Figure 7. It is noticeable that the Fe columns are right on top of the Ba or Ti columns at the coherent region. Moreover, it is observed that the contrast around the misfit dislocation regions at the interface appears slightly dark, which indicated that either cation deficiency or sample thickness difference may exist in these regions. It is well known that HAADF mode provides incoherent images, which uses high angle scattering and leads to strong atomic number (Z) contrast. The intensity of atom columns directly reflects their mean square atomic number and increases monotonously with the increase in

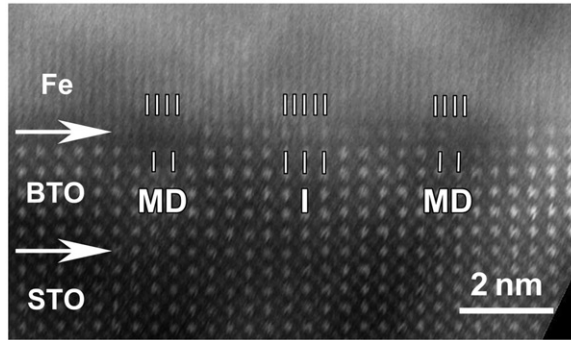


Figure 7. High-resolution Z-contrast image recorded along the [010] direction, showing the Fe/BTO interface structure with the registered and unregistered regions.

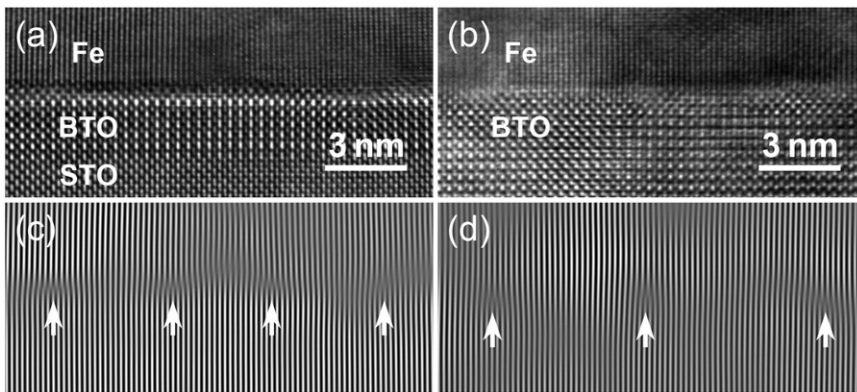


Figure 8. HRTEM lattice images at the Fe/BTO interface comparing the MD spacing in the films with the thickness of the BTO layer of (a) 2 nm and (b) 6 nm. Fourier filtered images shown in (c) and (d) correspond to the HRTEM image of (a) and (b), displaying the MD positions more clearly.

sample thickness. Preference thinning to areas with different structures during TEM specimen preparation may cause heavy disorder in the dislocation regions. From Figure 7, some atomic columns around dislocation regions are even missing, which could be understood from the viewpoint of imaging mode. It is proposed that defects may cause complications in HAADF image contrast formation by changing the interband transitions within the Bloch states and repopulating 1s states that have been exhausted by absorption [29]. The strain field of dislocations may result in the complete disorder of atom arrangements in areas around the dislocations, as is the case here.

3.3. Distance of the misfit dislocations at Fe/BaTiO₃ interface

The distance of the MDs observed above varies with the BTO thickness of the films. Figure 8a and b are [010] lattice images of the Fe/BTO interface area with the BTO

thickness below (2 nm) and above (6 nm) the critical thickness, respectively. To display the dislocations more clearly, the images are Fourier filtered by keeping only the Fourier components parallel to the interfaces, as shown in Figure 8c and d, respectively. From these two images, the MD spacings can be exactly measured. Obviously, the MD spacing in the films with totally strained 2-nm thick BTO is smaller than that in the films with partially relaxed 6-nm thick BTO. Using a statistical method, the distance of dislocations at the Fe/BTO interface for 2- and 6-nm thick BTO films was estimated to be 4.6 and 6.3 nm, respectively.

4. Discussion

4.1. Strain analysis in the Fe/BaTiO₃ thin films

The strain state and relaxation in Fe/BTO bilayer thin films on STO can be understood in the light of the film growth theory.

According to the film growth theory, an epitaxial interface will lose coherency and form a misfit dislocation for strain release if the films exceeds a critical thickness. It has been widely accepted that the critical thickness can be calculated using the Matthews–Blakeslee model [30,31]. In this model, mechanical equilibrium is established when the tension in the dislocation line balances the force exerted on the dislocation line by misfit stress. Thus, the formula for the critical thickness h_c is derived as:

$$h_c = \frac{b(1 - \nu \cos^2 \theta)}{8\pi f(1 + \nu) \cos \lambda} \left[\ln \left(\frac{\alpha h_c}{b} \right) + 1 \right]$$

Here, b is the length of the Burgers vector, θ is the angle between the dislocation line and its Burgers vector, λ is the angle between the slip direction and the direction in the film plane perpendicular to the line of intersection of the slip plane and the interface, f is the misfit of the interface, ν is the average Poisson ratio of the film and the substrate, and α is the cut-off radius of the dislocation core, where generally $1 < \alpha < 4$.

To facilitate assessing the extent of the strain relaxation of each layer and misfit dislocation formation at each interface in our Fe/BTO heterostructure films grown on STO substrates, the Matthews–Blakeslee formula was applied to calculate the critical thickness for two ideal situations, i.e. BTO film on STO substrate, and Fe layer on BTO bulk. The results are summarised in Table 1.

Table 1. Critical thickness calculated according to the Matthews–Blakeslee model for BTO films on a STO substrate and Fe films on a BTO substrate. In the calculation, the cut-off radius values of the dislocation core α range from 1 to 4.

Film/substrate	h_c (nm)
BTO/STO	2.6–4.6
Fe/BTO	2.1–3.3

For the system of BTO film on STO, Suzuki et al. [31] proposed the predominant MD formation mechanism of half-loop introduction by glide of pure edge dislocations on $\{101\}$ slip planes with Burgers vectors of type $a\langle 101 \rangle$, and listed experimental proof of this mechanism. They observed the dislocation with a Burgers vector of $a\langle 101 \rangle$ dissociated into $a\langle 100 \rangle$ and $a\langle 001 \rangle$ edge interfacial dislocations at the interface. The $a\langle 001 \rangle$ dislocations do not contribute to the misfit relaxation and are annihilated kinetically. Based on the Matthews–Blakeslee model, they estimated the critical thickness of this system as ~ 3 nm. In our calculation, a similar MD formation mechanism was assumed, and the same value of critical thickness was achieved, as shown in Table 1. Experimentally, it has been reported that the critical thickness of BTO film on STO lies between 2 and 4 nm by observing the dislocation formation process using TEM [31,32], which agrees well with the Matthews–Blakeslee model. However, in an epitaxial bilayer system, the strain relaxation of the lower layer is generally considered to be influenced by misfit with the upper layer [30,33]. Specifically, in the case of a Fe/BTO bilayer on STO, as the strain in the two layers is simultaneously compressive, it would be energetically favourable to relax the strains in both layers. Nevertheless, our result seems to follow the rules of BTO single films on STO. According to the results from the EDPs and HRTEM images presented above, the BTO layer starts to form misfit dislocation and relaxes the strain when its thickness is up to 3 nm. Therefore, the growth of an epitaxial Fe layer on top of BTO does not influence dislocation formation at the BTO/STO interface. This occurs probably because the growth temperature of the Fe layer (200°C) is too low for dislocation glide in the BTO layer or because the misfit strain in the top layer is mainly relaxed at the upper interface.

For the system of a Fe film on unstrained BTO, we assumed the misfit half-loop to be edge dislocations with Burgers vectors of type $\frac{a_{Fe}}{2}\langle 111 \rangle$ gliding on the $\{112\}_{Fe}$ planes in the Fe layer in our calculation. Similar to the case of the BTO layer on STO, the $\frac{a_{Fe}}{2}\langle 001 \rangle$ component of the Burgers vector of the dislocation perpendicular to the interface may be annihilated kinetically, leaving the $\frac{a_{Fe}}{2}\langle 110 \rangle$ component of the Burgers vector at the interface. This agrees with our experimental results above, showing the edge dislocations with the Burgers vectors of $\frac{a_{Fe}}{2}\langle 110 \rangle$ at the Fe/BTO interface, as determined by HRTEM. Our theoretical calculation indicates that its critical thickness is 2–3 nm. In our films, the thickness of the Fe layer is about 10 nm, far beyond the theoretical critical thickness. Moreover, the residual strain in the BTO layer induced by the STO substrate increases the lattice mismatch between Fe and BTO, which will make the Fe/BTO interface lose coherency more easily. Therefore, a misfit dislocations network is formed at the Fe/BTO interface and, thus, the Fe layers are relaxed to a large extent.

4.2. The configuration of the misfit dislocation network

In general, the dislocation network can be completely characterised by a combination of the Burger vectors \mathbf{b}_i and the line directions \mathbf{l}_i , i.e. $\{\mathbf{b}; \mathbf{l}\}$. The dislocation network observed at the (001) Fe/BTO interface is $\{\frac{a}{2}\langle 100 \rangle; \langle 010 \rangle\}$. To better understand the formation mechanism of the dislocation network, the coincidence site lattice (CSL) theory [34] was applied. Figure 9a shows a plan-view illustration of a

purely geometrical interface model. The atoms with different colours in the Fe lattice represent those at different height levels in the [001] direction. The black solid circles denote the positions where the first layer of Fe atoms is located exactly on top of the Ba and O atoms in the BTO lattice (Model A), while the black dashed circles denote the positions where the first layer of Fe atoms is located exactly above the hollow sites of the Ba and Ba atoms (Model B). The translation vector changing from Model A to Model B is $\frac{a}{2}\langle 100 \rangle$.

According to the CSL theory, the pattern of two-dimensional Wigner/Seitz cells around the coincidence site with the lowest interface energy predicts the network of edge-type dislocations. Because there is insufficient data showing whether model A or model B has the lowest energy, we attempted different ways to resolve this problem. Here, we follow the model suggested by Trampert et al. [35]. First, we

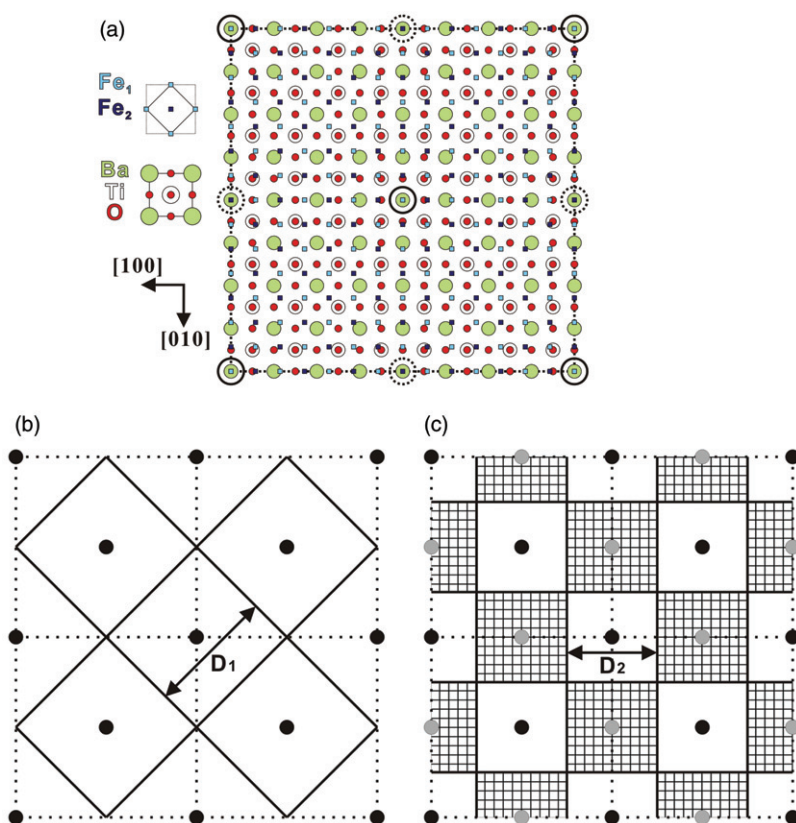


Figure 9. (a) Plan-view of the purely geometrical interface model for the Fe/BTO interface. The circles with black solid lines and dashed lines denote coincidence site positions of two types of interface. (b) The coincidence site lattice (CSL_1) consisted of only one type of interface, and the dislocation network N_1 it predicted. (c) The coincidence site lattice (CSL_2) consisted of both two types of interface, and the dislocation network N_2 it predicted. The area depicted in (b) and (c) is four times larger than that depicted in (a) for convenience. D_1 and D_2 in (b) and (c) denote the equilibrium MD spacings in network N_1 and N_2 .

assume one model has an obviously lower interface energy than the other model. Then, the solid lined circles (or the dashed lined circles) in Figure 9a constitute the pattern of CSL₁, as shown in Figure 9b. As a result, the edge of the Wigner/Seitz cells predicts the dislocation network $N_1 = \{\frac{a}{2}\langle 110\rangle; \langle 1\bar{1}0\rangle\}$, as drawn by black solid lines in Figure 9b. However, our experimental results disagree with this network N_1 . Then, we assume that the two interface models have approximately equivalent interfacial energy. Then, all the solid lined circles and dashed lined circles in Figure 9a constitute the patterns of CSL₂, which leads to the dislocation network $N_2 = \{\frac{a}{2}\langle 100\rangle; \langle 010\rangle\}$, as denoted by black solid lines in Figure 9c. This network agrees well with our experimental observations. Each dislocation in network N_2 is a partial dislocation, which introduce the translation state on two sides of the dislocations. In other words, the pattern of “Fe on top of Ba and O” coincidence points is extended by those points where Fe positions are located exactly above the hollow positions between Ba and Ba atoms (checked squares in Figure 9c). Therefore, two types of interface are distributed alternatively and make up a chessboard pattern, as shown with alternative blank squares and checked squares in Figure 9c.

Trampert et al. [35] discussed this phenomenon when they studied the dislocation network in an Ag/MgO interface. Recently, the Cu/MgO interface was observed to have a similar misfit dislocation network using Cs-corrected HRTEM [36]. In fact, network N_2 exists in a more general situation. This phenomenon can be understood from the energy balance between the dislocation energy and the interfacial energy. The total dislocation energy E_d can be written as:

$$E_d = E_0 b^2 \cdot l$$

Here, l is the total length of the dislocation lines. E_d for network N_1 in one CSL₁ cell is $E_0 a D_1$, higher than E_d for network N_2 in the same area ($\frac{\sqrt{2}}{2} E_0 a D_1$). The energy gained from E_d compensates the formation energy of the high energy interface area when changing from network N_1 to network N_2 . Therefore, network N_2 will be more energetically favourable than network N_1 , if the difference of the interfacial energies of the two models is not large or if the misfit dislocation density is very large.

Based on the results of EDPs and the discussion of strain, due to different degree of strain relaxation states when the BTO layers thicknesses are below or above the critical thickness, the lattice constants of the BTO layers are different. Then, the lattice mismatches between Fe and BTO are different for each film, as shown in Table 2. The geometrically expected equilibrium spacings D of the MDs at the Fe/BTO interface were theoretically estimated based on the equation $D = b/f$.

Table 2. Summary of the theoretical equilibrium and experimental MD spacing in the dislocation network at the Fe/BTO interface with variations in BTO thickness of the films.

BTO thickness of the films (nm)	Average lattice mismatch (%)	Theoretical equilibrium MD spacing (nm)	MD spacing in this experiment (nm)
2	-4.3	4.7	4.6 ± 0.4
6	-3.0	6.8	6.3 ± 0.6

It was found that the spacing of the MDs for Fe/BTO with a 2-nm thick BTO is 4.7 nm; whereas that for Fe/BTO with a 6-nm thick BTO is 6.8 nm, which agree well with the experimental HRTEM data presented above of 4.6 and 6.3 nm, respectively. A comparison of the theoretical equilibrium and experimental MD spacings for films with different BTO thicknesses are summarised in Table 2.

5. Conclusions

The epitaxial growth of Fe films on high quality BTO films and the magnetoelectric epitaxial interface of Fe/BTO were achieved by delicate control of both PLD and magnetron sputtering. From electron diffraction patterns, the epitaxial relationships between Fe and BTO films are determined to be $(001)_{\text{Fe}} \parallel (001)_{\text{BTO}}$ and $[\bar{1}10]_{\text{Fe}} \parallel [010]_{\text{BTO}}$, in accordance with the assumptions in early first principles calculations on the Fe/BTO interface. Our work provides direct evidence for the rationality of the atomic model on which the theoretical calculations are based and for the possibility of studying magnetoelectric coupling in this kind of interface.

The strain states in the films and interface defects at the Fe/BTO interface are investigated by TEM. The main interface defects are misfit dislocations with the form of square networks. Their Burgers vectors are determined to be $\frac{1}{2}a\langle 100 \rangle$, and their line directions are type $\langle 010 \rangle$. These dislocations are partial dislocations, and are able to change the translation state of the Fe/BTO interface. Therefore, two types of interface model coexist at the interface. The MD spacings in the dislocation network are considerably influenced by the thickness of the BTO films. The observed structure and defects of the Fe/BTO interface may lead to a realistic prediction of interfacial magnetoelectric coupling and an improved intentional design of the interface by controlling the misfit strain and interfacial defects.

Acknowledgements

This work was supported by the National Basic Research Program of China (2009CB623705 and 2010CB631206), and the National Natural Science Foundation of China (No. 50871115 and No. 51171190).

References

- [1] N.A. Spaldin and M. Fiebig, *Science* 309 (2005) p.391.
- [2] G. Catalan and J.F. Scott, *Adv. Mater.* 21 (2009) p.2463.
- [3] M. Fiebig, T. Lottermoser, D. Frohlich, A.V. Goltsev and R.V. Pisarev, *Nature* 419 (2002) p.818.
- [4] N. Ikeda, H. Ohsumi, K. Ohwada, K. Ishii, T. Inami, K. Kakurai, Y. Murakami, K. Yoshii, S. Mori, Y. Horibe and H. Kito, *Nature* 436 (2005) p.1136.
- [5] T. Kimura, T. Goto, H. Shintani, K. Ishizaka, T. Arima and Y. Tokura, *Nature* 426 (2003) p.55.
- [6] H. Schmid, *J. Phys.: Condens. Matter.* 20 (2008) p.434201.
- [7] L.W. Martin, Y.H. Chu and R. Ramesh, *Mater. Sci. Eng. R* 68 (2010) p.89.

- [8] T. Zhao, A. Scholl, F. Zavaliche, K. Lee, M. Barry, A. Doran, M.P. Cruz, Y.H. Chu, C. Ederer, N.A. Spaldin, R.R. Das, D.M. Kim, S.H. Baek, C.B. Eom and R. Ramesh, *Nat. Mater.* 5 (2006) p.823.
- [9] D. Lebeugle, D. Colson, A. Forget, M. Viret, A.M. Bataille and A. Gukasov, *Phys. Rev. Lett.* 100 (2008) p.227602.
- [10] B. Lorenz, Y.Q. Wang, Y.Y. Sun and C.W. Chu, *Phys. Rev. B* 70 (2004) p.212412.
- [11] H. Zheng, J. Wang, S.E. Lofland, Z. Ma, L. Mohaddes-Ardabili, T. Zhao, L. Salamanca-Riba, S.R. Shinde, S.B. Ogale, F. Bai, D. Viehland, Y. Jia, D.G. Schlom, M. Wuttig, A. Roytburd and R. Ramesh, *Science* 303 (2004) p.661.
- [12] X. Lu, Y. Kim, S. Goetze, X. Li, S. Dong, P. Werner, M. Alexe and D. Hesse, *Nano Lett.* 11 (2011) p.3202.
- [13] I. Vrejoiu, M. Ziese, A. Setzer, P. Esquinazi, B. Birajdar, A. Lotnyk, M. Alexe and D. Hesse, *Appl. Phys. Lett.* 92 (2008) p.152506.
- [14] J.P. Velev, S.S. Jaswal and E.Y. Tsybal, *Philos. Trans. R. Soc. A* 369 (2011) p.30699.
- [15] C.G. Duan, S.S. Jaswal and E.Y. Tsybal, *Phys. Rev. Lett.* 97 (2006) p.047201.
- [16] M. Fechner, I.V. Maznichenko, S. Ostanin, A. Ernst, J. Henk, P. Bruno and I. Mertig, *Phys. Rev. B* 78 (2008) p.212406.
- [17] T.Y. Cai, S. Ju, J. Lee, N. Sai, A.A. Demkov, Q. Niu, Z.Y. Li, J.R. Shi and E.G. Wang, *Phys. Rev. B* 80 (2009) p.140415.
- [18] J. Lee, N. Sai, T.Y. Cai, Q. Niu and A.A. Demkov, *Phys. Rev. B* 81 (2010) p.144425.
- [19] V. Garcia, M. Bibes, L. Bocher, S. Valencia, F. Kronast, A. Crassous, X. Moya, S. Enouz-Vedrenne, A. Gloter, D. Imhoff, C. Deranlot, N.D. Mathur, S. Fusil, K. Bouzehouane and A. Barthelemy, *Science* 327 (2010) p.1106.
- [20] S. Brivio, C. Rinaldi, D. Petti, R. Bertacco and F. Sanchez, *Thin Solid Films* 519 (2011) p.5804.
- [21] H.L. Meyerheim, F. Klimenta, A. Ernst, K. Mohseni, S. Ostanin, M. Fechner, S. Parihar, I.V. Maznichenko, I. Mertig and J. Kirschner, *Phys. Rev. Lett.* 106 (2011) p.087203.
- [22] Y.S. Kim, D.H. Kim, J.D. Kim, Y.J. Chang, T.W. Noh, J.H. Kong, K. Char, Y.D. Park, S.D. Bu, J.G. Yoon and J.S. Chung, *Appl. Phys. Lett.* 86 (2005) p.102907.
- [23] C.L. Jia, M. Siegert and K. Urban, *Acta Mater.* 49 (2001) p.2783.
- [24] S.H. Oh, C. Scheu, T. Wagner, E. Tchernychova and M. Ruhle, *Acta Mater.* 54 (2006) p.2685.
- [25] X. Wang, Y.L. Zhu, M. He, H.B. Lu and X.L. Ma, *Acta Mater.* 59 (2011) p.1644.
- [26] Y.L. Zhu, X. Wang, M.J. Zhuo, Y.Q. Zhang and X.L. Ma, *Philos. Mag. Lett.* 90 (2010) p.323.
- [27] T. Zhao, F. Chen, H.B. Lu, G.Z. Yang and Z.H. Chen, *J. Appl. Phys.* 87 (2000) p.7442.
- [28] C. Wang, B.L. Cheng, S.Y. Wang, H.B. Lu, Y.L. Zhou, Z.H. Chen and G.Z. Yang, *Thin Solid Films* 485 (2005) p.82.
- [29] P.D. Nellist and S.J. Pennycook, *Adv. Imag. Electron Phys.* 113 (2000) p.148.
- [30] J.W. Matthews and A.E. Blakeslee, *J. Cryst. Growth* 27 (1974) p.118.
- [31] T. Suzuki, Y. Nishi and M. Fujimoto, *Philos. Mag. A* 79 (1999) p.2461.
- [32] H.P. Sun, W. Tian, X.Q. Pan, J.H. Haeni and D.G. Schlom, *Appl. Phys. Lett.* 84 (2004) p.3298.
- [33] Y.B. Chen, H.P. Sun, M.B. Katz, X.Q. Pan, K.J. Choi, H.W. Jang and C.B. Eom, *Appl. Phys. Lett.* 91 (2007) p.252906.
- [34] W. Bollman, *Crystal Defects and Crystalline Interfaces*, Springer, Berlin, 1970.
- [35] A. Trampert, F. Ernst, C.P. Flynn, H.F. Fischmeister and M. Ruhle, *Acta Metall. Mater.* 40 (1992) p.S227.
- [36] S. Cazottes, Z.L. Zhang, R. Daniel, J.S. Chawla, D. Gall and G. Dehm, *Thin Solid Films* 519 (2010) p.1662.